Research Square

Preprints are preliminary reports that have not undergone peer review.
They should not be considered conclusive, used to inform clinical practice,
or referenced by the media as validated information.

Exploratory Proteomics and Radiomics Correlates of [68Ga]Ga-ABY-025 PET Uptake in HER2-Low Metastatic Breast Cancer: A Pilot Study

Konstantinos Vrettos
Artificial Intelligence and Translational Imaging (ATI) Lab, Department of Radiology, School of Medicine, University of Crete, Heraklion

Henrik Johansson
SciLifeLab

Mahshid Zarrineh
SciLifeLab

Luca Finn Gaessler
SciLifeLab

Janne Lehtiö
SciLifeLab

Siri Af Buren
Karolinska Institute: Karolinska Institutet

Ted Nilsson
Karolinska Institute: Karolinska Institutet

Maria Holstensson
Karolinska University Hospital: Karolinska Universitetssjukhuset

Thuy Tran
Karolinska Institute: Karolinska Institutet

Rimma Axelsson
Karolinska Institute: Karolinska Institutet

Elisavet Vallera
Protavio Ltd, Demokritos Science Park, Athens

Michail E Klontzas
Karolinska Institute: Karolinska Institutet

Antonios Tzortzakakis
Karolinska Institute: Karolinska Institutet

Renske Altena
renske.altena@ki.se

Karolinska Institute: Karolinska Institutet https://orcid.org/0000-0001-6944-5209

Research Article

Keywords:

Posted Date: November 12th, 2026

DOI: https://doi.org/10.21203/rs.3.rs-11420781/v1

License: This work is licensed under a Creative Commons Attribution 4.0 International License.
Read Full License

Exploratory Proteomics and Radiomics Correlates of [^{68}Ga]Ga-ABY-025 PET Uptake in HER2-Low Metastatic Breast Cancer: A Pilot Study

Short title: Multi-omics in HER2-low breast cancer

Konstantinos Vrettos[1], Henrik J. Johansson[2], Mahshid Zarrineh[2], Luca Finn Gaessler[2], Janne Lehtiö[2,3], Siri af Burén[4,5], Ted Nilsson[4], Maria Holstensson[4,5], Thuy A. Tran[2,6], Rimma Axelsson[5,7], Elisavet Vallera[8], Michail E. Klontzas[1,4,9], Antonios Tzortzakakis[4,5], Renske Altena[2]

Author affiliations:

[1]Artificial Intelligence and Translational Imaging (ATI) Lab, Department of Radiology, School of Medicine, University of Crete, Heraklion, Greece

[2]Department of Oncology-Pathology, Karolinska Institutet and Science for Life Laboratory, Stockholm, Sweden

[3]Clinical Proteomics Unit, Karolinska University Hospital, Stockholm, Sweden

[4]Division of Radiology, Department of Clinical Science, Intervention and Technology (CLINTEC), Karolinska Institutet, Stockholm, Sweden

[5]Medical Radiation Physics and Nuclear Medicine, Functional Unit of Nuclear Medicine, Karolinska University Hospital, Huddinge, Sweden

[6]Department of Radiopharmacy, Karolinska University Hospital, Solna, Sweden

[7]Department of Molecular Medicine and Surgery, Karolinska Institutet, Stockholm, Sweden

[8]Protavio Ltd, Demokritos Science Park, Athens, Greece

[9]Computational BioMedicine Laboratory, Institute of Computer Science, Foundation for Research and Technology Hellas (FORTH), Heraklion, Greece

* Correspondence: Renske Altena MD PhD, Department of Oncology-Pathology, Karolinska Institutet, Stockholm Sweden, Email: renske.altena@ki.se, Telephone: +46 72 844 94 85.

Key points

- This work combines CT radiomics ([^{68}Ga]Ga-ABY-025 PET/CT) with proteomics (tumor biopsy), in addition to gold standard immunohistochemistry
- In patients with HER2-low tumors, neither IHC scores nor SUVmax correlated with the total expressed HER2 (ERBB2) by proteomics analysis.
- SUVmax correlated with a set of proteins involved in membrane composition, endocytic recycling and cytoskeletal remodeling, rather than total HER2 quantity, which may help explain PET-IHC discordance in HER2-low patients.
- Proposed mechanism for why SUVmax does not correlate with total HER2 abundance.
- Radiomics features (wavelet) showed near-perfect rank correlations ($|r_s| = 1.0$) with ERBB2 levels (HER2), a hypothesis-generating finding, that requires independent validation before it can be considered a non-invasive biomarker.

Abstract

Background

Human epidermal growth factor receptor 2 (HER2)-low metastatic breast cancer is now an actionable subtype, yet patient selection remains challenging. The aim of this work was to investigate whether multi-omics profiling (proteomics and radiomics) of paired tumor biopsies could explain the observed discordance between PET uptake, IHC score and total HER2 abundance.

Methods

Ten patients with HER2-low metastatic breast cancer underwent [^{68}Ga]Ga-ABY-025 PET/CT and tumor biopsy in a pilot clinical trial. Discovery proteomics quantified 5,341 proteins in eight patients, and CT radiomics extracted 2,046 features from nine patients (seven with both). Multi-Omics Factor Analysis (MOFA), Spearman correlations, and Enrichr pathway/transcription-factor enrichment were performed.

Results

Total ERBB2 (HER2) protein abundance did not correlate with SUVmax (Spearman $r_s = 0.19$, $P = 0.65$). MOFA suggested a separation of the radiomics-linked latent factor (LF1) associated with HER2 (ERBB2) abundance from a proteomics-linked factor (LF3) associated with SUVmax. Top SUVmax-correlated proteins included AGPS (membrane composition), ARHGDIA (cytoskeletal remodeling) and ATAD1 (membrane protein quality control) (Spearman $r \geq 0.95$). Enrichment of positive correlates implicated vesicle-mediated transport (adjusted $P = 0.0024$), endocytic recycling (adjusted $P = 0.0087$), peroxisomal function (adjusted $P = 0.0015$) and focal adhesion (adjusted $P = 0.0007$). Specific radiomics features, such as wavelet-HLL_firstorder_Minimum, correlated well with HER2 levels ($r_s > 0.95$) ; however, none remained statistically significant after correction for multiple comparisons in this small cohort.

Conclusion

In this hypothesis-generating analysis, PET uptake aligned with membrane-microenvironment proteins, rather than with total HER2 abundance. These findings are consistent with a model in which [^{68}Ga]Ga-ABY-025 uptake reflects cell-surface HER2 availability influenced by membrane trafficking, cytoskeletal organization, and endocytic recycling, and identify candidate biomarkers and radiomic signatures for validation in larger cohorts.

Trial registration: Clinicaltrials.gov, NCT05619016, https://clinicaltrials.gov/study/NCT05619016. Date of registration Nov 30th 2022.

Introduction

Human epidermal growth factor receptor 2 (HER2) is a key biomarker in breast cancer that guides the use of targeted therapies. The traditional binary classification of HER2-positive versus HER2-negative has been shifted by the recognition that a substantial proportion of patients express (ultra-) low levels of HER2 (HER2-low: IHC 1+ or 2+ without gene amplification; HER2-ultralow: faint membrane staining), now termed HER2-low and HER2-ultralow breast cancer [1][2]. The approval of the HER2-targeted antibody-drug conjugate trastuzumab deruxtecan (T-DXd) for HER2-low and HER2-ultralow advanced and metastatic breast cancer (mBC) based on the DESTINY-Breast04 and DESTINY-Breast06 trials [3] [4] has expanded therapeutic options for a large share of patients with mBC. However, sensitive and reliable therapy-predictive biomarkers for the benefit of Trastuzumab deruxtecan (T-DXd) in patients with HER2-low and HER2-ultralow mBC are still missing [5].

This may partly be explained because HER2 expression is spatially [7] and temporally heterogeneous [8]. Tissue biopsy, the current gold standard, is limited by its invasiveness, sampling error and impracticality for whole-body or longitudinal assessment [9]. A single biopsy from one metastatic lesion may not reflect the total disease burden, as up to 40% of patients have varied HER2 expression between primary tumor and metastases [10]. Moreover, suboptimal inter-pathologist reproducibility for HER2-low scoring has been documented [11][12] and earlier works have questioned the ability of IHC to accurately predict T-DXd antitumor activity [5].

Contrary to IHC, HER2-targeted [^{68}Ga]Ga-ABY-025 PET/CT enables real-time, whole-body assessment of HER2 expression, and several tracers have been clinically evaluated [13][14]. ABY-025 is a small (~7 kDa) engineered affibody molecule that binds a unique epitope on Domain III of the HER2 extracellular domain [15] and does not compete with pertuzumab (Domain II binder) [15] or trastuzumab (Domain IV binder [16]). Previously, our group demonstrated, in the patient sample that forms the basis for the current work, that [^{68}Ga]Ga-ABY-025 PET/CT in patients with HER2-low mBC revealed substantial intra- and interindividual heterogeneity in tracer uptake (SUVmax in biopsied lesions ranged from 3.7 to 33.4) [17]. A subsequent systematic review of 10 reports comprising 195 lesions confirmed moderate-to-good lesion-level concordance between HER2 PET uptake and biopsy grade, with most "false-positive" lesions being HER2-low rather than HER2-zero, supporting a continuum model of HER2 expression [13]. Consequently, the relationship between [^{68}Ga]Ga-ABY-025 uptake and IHC score warrants further investigation.

To date and to the best of our knowledge, no study, for HER2-targeted tracers or for any other class of PET radiotracer, has investigated whether in vivo PET tracer uptake correlates with unbiased discovery multi-omics in paired tumor biopsies. This exploratory, hypothesis-generating study, using material from our previously published HER2-PET pilot trial in HER2-low metastatic breast cancer, was designed to close that gap. The aim was to investigate why PET-derived HER2 signal and IHC can disagree by identifying the molecular and microenvironmental features underlying it. In the case of HER2-low in particular, where IHC is

poorly reproducible [11] yet used to gate access to T-DXd [6], understanding the biological basis of [^{68}Ga]Ga-ABY-025 PET and IHC discordance could inform patient selection for T-DXd treatment. This work explored correlations between proteomics analyses on tumor biopsies and radiomics features from the corresponding lesions in conjunction with the gold standard IHC.

Materials and Methods

Study Design and patient population

This analysis was performed on tumor biopsies and [^{68}Ga]Ga-ABY-025 PET/CT from a prospective pilot study of HER2-low metastatic breast cancer (mBC)(EU CT 2022-500448-39-00; ClinicalTrials.gov NCT05619016), conducted as part of an ongoing phase II single-center basket imaging study with [^{68}Ga]Ga-ABY-025. Detailed ethics, eligibility criteria, patient characteristics, HER2 PET/CT acquisition protocols, biopsy procedures, and clinical outcomes were published previously [17]. Tumor-to-background ratio (TBR) was calculated as lesion SUVmax divided by mean splenic SUV. In brief, 10 patients with previously biopsy-verified HER2-low disease (IHC 1+ or 2+ without HER2 gene amplification) underwent [^{68}Ga]Ga-ABY-025 PET/CT in conjunction with tumor biopsy. Eight patients had adequate proteomics data available for analysis. Nine had evaluable radiomics segmentations, and seven had overlapping data for both modalities. Patient 6 contributed two replicate biopsy samples obtained from the same lesion, which were averaged for the primary analysis. Patient 8 had a liver biopsy obtained 28 days before PET imaging that was deemed representative since no systemic cancer therapy was administered in the interim. The study was approved by the Swedish Medical Product Agency and the Ethical Review Authority (Dnr 5.1-2022-58345), and all participants provided written informed consent. Two patients had HER2 IHC 0 on their study-specific biopsy (Patient 6, skin lesion; Patient 5, liver metastasis) despite prior HER2-low–qualifying biopsies (Patient 6, breast/skin IHC 1+; Patient 5, primary tumor IHC 2+), reflecting the well-documented spatial and temporal heterogeneity of HER2 expression across metastatic lesions.

Proteomics: Sample Processing and Mass Spectrometry

Formalin-fixed paraffin-embedded (FFPE) tumor biopsy tissue was processed for discovery mass spectrometry-based proteomics using liquid chromatography–tandem mass spectrometry (LC-MS/MS). For each sample, 6 sections of 5-µm-thick FFPE tissue sections were collected and transferred into low-binding microcentrifuge tubes for protein extraction.

Approximately 200 µL of lysis buffer containing 4% (w/v) sodium dodecyl sulfate (SDS), 200 mM dithiothreitol (DTT), and 200 mM Tris-HCl (pH 8.0) was added to each sample. Samples were incubated at 90 °C for 30 min and subsequently subjected to probe sonication using an ultrasonic processor (UP200ST, Hielscher Ultrasonics, Germany) at 100% amplitude with a

70% pulse cycle for 15 min. Samples were then incubated again at 90 °C for 15 min, followed by a second sonication step at 100% amplitude and a 70% pulse cycle for 7.5 min.

Protein extracts were purified using the single-pot, solid-phase-enhanced sample preparation (SP3) method with Sera-Mag SpeedBeads Carboxyl Magnetic Beads, including hydrophobic beads (Cytiva; cat#11819912), and hydrophilic beads (Cytiva; cat#11548692, Fisher Scientific) following described protocol. Following protein cleanup, samples were reduced and digested on SP3 beads using 2 µg of RapiZyme Trypsin MS Grade (Waters, Milford, USA; cat#186010108-1) per sample as fix digestion enzyme amount, overnight in 37°C.

Following enzymatic digestion, peptides were subjected to an additional SP3-based cleanup and subsequently aliquoted for LC–MS/MS analysis. All SP3 cleanup, reduction, and digestion steps were performed using a Biomek i7 automated liquid-handling workstation (Beckman Coulter Life Sciences, USA).

All nine proteomics samples were processed within the same lysis and sample-processing batch to minimize technical variation arising from sample preparation.

Mass spectrometry analysis

For LC–MS/MS measurements, 500 ng of peptide was loaded to Evotip PURE (EV2013, Evosep) and processed in accordance with the manufacturer's protocol. The LC separation was conducted on an Evosep operated in the 30 samples per day (30SPD) mode. A PepSep FIFTEEN analytical column (15 cm × 150 µm × 1.5 µm; Bruker, 1893474) was used for peptide separation and was maintained at 40°C. Electrospray ionization was achieved using a 20 µM ZDV Sprayer (Bruker, 1865710).

Peptide ions were analyzed with a Bruker timsTOF HT mass spectrometer. The ionization source was operated at 1500 V with a dry gas flow of 3 L/min and a drying temperature of 180°C. Fragmentation energy was adjusted according to ion mobility, ranging from 15 eV at the ion mobility of $1/K_0$ = 0.60 V·s/cm^2 to 70 eV at $1/K_0$ = 1.60 V·s/cm^2.

The instrument was operated in diaPASEF mode with range of between 300 and 1300 for m/z and within the ion mobility interval of 0.6–1.6 $1/K_0$. The diaPASEF method isolate precursors in 16 dia-PASEF windows optimized with the Py-DiaId Python package (Skowronek et al., 2022) using the Bruker human spectral library. Ion accumulation and fragmentation were coordinated within each acquisition cycle, resulting in a total cycle duration of 1.8 s.

Proteomic data processing and quantification

Following acquisition, the resulting files were seached using Spectronaut version 20.1 (Biognosys, Switzerland) for label-free proteome analysis. Data processing was performed with the directDIA+ (Deep) workflow. Peptide-spectrum matching was carried out using the Pulsar search engine against the human reference proteome from Ensembl v114. Cysteine carbamidomethylation was defined as a static modification, oxidation of methionine and acetylation at the protein N-terminus were allowed as variable modifications.

Identification confidence was controlled by applying a 1% FDR threshold to peptide and precursor identifications. An additional 1% FDR criterion was applied at the experiment level for protein groups. The analysis incorporated dynamic mass tolerances for both MS1 and MS2 data, together with automated calibration of chromatographic retention times.

Quantitative analysis was based on MS2-derived signal intensities. To account for differences between LC–MS runs, global median normalization was applied before protein-level quantification. Protein quantities were subsequently inferred using MaxLFQ, restricting the analysis to peptides uniquely attributable to individual genes. For each protein, the quantification procedure incorporated no more than three peptide groups, with a maximum of six precursor ions considered within each peptide group.

Raw data were converted to comma-separated values and filtered to retain proteins detected in all samples (complete-case analysis), yielding 5,341 proteins for downstream analysis. Per-sample missingness prior to filtering ranged from 15.4% to 26.4%. For visualization and dimensionality reduction, abundances were log2-transformed and row-wise Z-score normalized.

Radiomics Extraction and Processing

Three-dimensional radiomics features were extracted from co-registered contrast-enhanced CT scans obtained during the [^{68}Ga]Ga-ABY-025 PET/CT examination. The biopsy sites were identified, and corresponding Regions of Interest (ROIs) were defined on the CT scans by a senior radiologist who is also a certified nuclear medicine physician. Feature extraction was performed using PyRadiomics following the recommendations of ESR and EuSoMII [18], yielding 2,046 features. Features were standardized using standard scaling across all patients. The radiomics cohort comprised nine patients with available segmentations; for analyses overlapping with proteomics, the cohort was restricted to seven

Multi-Omics Factor Analysis (MOFA)

To integrate the high-dimensional proteomics (5,341 features) and radiomics (2,046 features) views in an unsupervised, multi-modal framework, Multi-Omics Factor Analysis (MOFA) was performed using the `mofapy2` python package. MOFA generalizes Principal Component Analysis (PCA) to multi-view data, decomposing each observed matrix into a product of patient-specific (latent) factor scores and data-specific loadings, plus residual noise.

The primary motivation for using MOFA was to identify orthogonal axes of joint variation that could distinguish (a) absolute tissue receptor density, from (b) the functional cellular machinery governing surface receptor presentation and in vivo tracer binding, which we hypothesized would be reflected in the broader proteomics landscape and in vivo PET tracer uptake.

Because patients with missing views (Patient 6 missing radiomics, Patients 4 and 5 missing proteomics) still contain valuable covariance information, MOFA's probabilistic framework utilizes them during training by marginalizing over missing values [19][20]. In contrast to complete-case analysis, this approach leverages all observed entries to infer the shared latent factors and has been shown to yield more robust inference in sparse multi-modal data [20]. We trained the model on the full cohort (N=10) and evaluated factor correlations across the matched subset (N=7) with complete data for both modalities. Factor interpretation was performed by calculating Spearman rank correlations between latent factor scores and clinical metrics (SUVmax, TBR, IHC score, HER2 proteomics) and by inspecting data-specific loadings (weights) for proteins and radiomics features.

Discovery Correlation and Pathway Analyses

To biologically interpret the MOFA latent factors and identify specific molecular drivers, we performed post-hoc correlation analyses. Spearman rank correlations were calculated between protein expression and PET metrics (SUVmax, TBR) across the eight patients with proteomics data. Analogous correlations were calculated between radiomics features and clinical metrics (SUVmax, TBR, IHC, ERBB2 proteomics) across the available cohorts (nine patients). Multiple testing correction was performed using the Benjamini-Hochberg false discovery rate (FDR).. For proteome-wide testing, the Bonferroni threshold is additionally reported for reference as for n = 8 the smallest attainable exact two-sided Spearman P-value is 4.96×10^{-5}, which exceeds the Bonferroni threshold of 9.36×10^{-6}. Consequently, error control at the proteome-wide level is unattainable at this sample size by construction

Given the exploratory nature of this pilot study and limited statistical power (n=8 provides power = 0.325 to detect r = 0.95 at Bonferroni-corrected alpha with 5,341 tests), we emphasize effect sizes and confidence intervals (Fisher z-transformation) alongside corrected p-values. Effect sizes were interpreted according to Cohen's conventions (small: r = 0.10; medium: r = 0.30; large: r = 0.50).

To identify enriched biological pathways and transcriptional regulators associated with the SUVmax-linked proteomics axis, over-representation analysis (ORA) was conducted using the Enrichr API (Ma'ayan Laboratory) against Gene Ontology (GO) Biological Process 2023, GO Cellular Component 2023, KEGG 2021 Human pathways, and ENCODE/ChEA Consensus TFs from ChIP-X. Proteins with strong SUVmax correlations (absolute Spearman $r \geq 0.70$) were selected as input. Enriched terms were ranked by combined score ($c = \ln(p) \times z$, where p is the Fisher's exact test P-value and z is the z-score deviation from the expected rank) and filtered at Benjamini–Hochberg adjusted $P < 0.05$. All analyses were performed using Python 3.13 (pandas, numpy, scipy, seaborn, scikit-learn, mofapy2).

Results

Patient characteristics and quantitative PET measures

Table 1 summarizes details of the eight patients with complete proteomics data. The median age was 66 years (range, 57-74). SUVmax in the biopsied lesions ranged from 3.7 to 33.4 (median: 12.5), and TBR ranged from 1.7 to 15.9 (median:6.8). Substantial heterogeneity was observed both between and within patients. Patient 8, showed the highest SUVmax (33.4) and TBR (15.9) in the cohort.

Proteomics Quality Control

Mass spectrometry analysis yielded 9,540 proteins across the nine samples. After complete-case filtering, 5,341 proteins detected in all patients were retained. The two replicate samples from patient 6 showed high correlation in their protein expression profiles (Pearson r = 0.946, P < 0.001), confirming technical reproducibility and supporting the decision to average them for the primary analysis. Principal component analysis revealed that PC1 explained 23.1% of variance and separated samples primarily by hormone receptor status (ER-positive versus ER-negative). PC2 explained 17.8% of variance and highlighted individual patient heterogeneity, with patient 10 clustering separately due to extremely high ERBB2 and overall proteomics expression (Figure 1A). Hierarchical clustering of the top 100 most variable proteins showed distinct grouping patterns (Figure 1B).

ERBB2 Protein Abundance Does Not Correlate with [^{68}Ga]Ga-ABY-025 PET Uptake

Total ERBB2 (HER2) protein abundance measured by mass spectrometry showed no significant correlation with either SUVmax or TBR. Across the eight patients with proteomics data (averaging Patient 6 replicates), the total ERBB2 protein abundance ranged from 202.3 to 1424.1 (median: 479.3). The Spearman rank correlation between ERBB2 abundance and SUVmax was r_s = 0.1905 (95% CI, -0.594 to 0.789; P = 0.651). Correlations with TBR were also weak and non-significant (Spearman r_s = 0.3114, P = 0.453) (Table 2).

Two notable outliers contributed to this disconnect. Patient 8 had the highest [^{68}Ga]Ga-ABY-025 uptake in the cohort (SUVmax = 33.4) and HER2 IHC 2+, but relatively low ERBB2 protein abundance (294.4). Conversely, patient 10 had the highest ERBB2 abundance by a large margin (1,424.1), paired with IHC 2+, but average [^{68}Ga]Ga-ABY-025 uptake (SUVmax = 12.0, median: 12.5), possibly reflecting high cellular receptor density but limited overall lesion perfusion or macroscopic tracer binding.

Exploratory Multi-Omics Factor Analysis Identifies Separate Latent Factors for Receptor Density and Tracer Binding

To investigate why total ERBB2 abundance was not correlated with [^{68}Ga]Ga-ABY-025 uptake, the high-dimensional proteomics (5,341 features) and radiomics (2,046 features) datasets were integrated using MOFA across the cohort (N=10), evaluating factor correlations across the matched cohort (N=7, Patients 1, 2, 3, 7, 8, 9, 10). The model captured a cumulative variance of 43.8% in the proteomics view and 53.2% in the radiomics view (Figure 2). LF1 was heavily driven by radiomics (38.7% variance) and correlated with mass spectrometry-measured ERBB2 proteomics (r_s = 0.857, raw p = 0.014, FDR-corrected-p = 0.164, N=7), with ERBB2 loading positively on LF1 (weight = 0.1953) but near-zero on other factors (Table 3). In contrast, LF3 was predominantly proteomics (22.1% variance) and correlated with clinical PET SUVmax (r_s = 0.714, raw p = 0.071, FDR-corrected-p = 0.387, N=7) and TBR (r_s = 0.631, raw p = 0.129, FDR-corrected-p = 0.387, N=7), but was independent of ERBB2 (r_s = 0.107, P = 0.819, FDR-corrected-p = 0.912, N=7) (Figure 2B). While the proteins with the highest absolute LF3 loadings were primarily metabolic enzymes (e.g., FAHD2A) and protein regulatory factors (e.g.UBAC1) with modest univariate SUVmax correlations (Figure 2B), the identified regulators of membrane-associated processes and cytoskeletal remodeling (ARHGDIA (weight = 0.4749), ATAD1 (0.2677), AGPS (0.2463)) combined positive LF3 loading with strong SUVmax correlations (r ≥ 0.95) (Table 3, Figure 2D). Notably, none of the 12 factor–metric associations remained statistically significant after FDR correction (adjusted P < 0.05), which may in part reflect the limited statistical power associated with the small matched sample size (N = 7) and correction for multiple comparisons.

These results show that unsupervised integration separated a radiomics-linked factor (LF1, associated with ERBB2 abundance) from a proteomics-linked factor (LF3, associated with SUVmax and TBR). See Discussion for biological interpretation.

Proteomics Correlates of the SUVmax-Associated Latent Factor

Post-hoc analysis of the proteomics view revealed several proteins that showed strong positive correlations with SUVmax (Table 2). The top three proteins across all 5,341 features were ATAD1, VPS37A, and AGPS, each with identical Spearman rank correlations of r_s = 0.9762 (95% CI, 0.870 to 0.996). The next tier included NT5C and ARHGDIA (Spearman r_s = 0.9524; 95% CI, 0.753 to 0.992) (Figure 3). With n=8, Spearman's r is fixed by rank order, and only a limited number of distinct correlation values are achievable. Negatively correlated proteins included PSMD5 (r_s = -0.9286), SETMAR (r_s = -0.9286), and RRP15 (r_s = -0.9048), among others. Notably, several of these negatively correlated proteins are involved in ribosome biogenesis (RRP15, PES1) and proteasome assembly (PSMD5). The heatmap of the top 20 correlated proteins (10 positive, 10 negative), sorted by patient SUVmax, presents the expression of the most strongly positively and negatively correlated proteins across the patient

cohort (Figure 3C). To place these selected proteins in the context of the full proteome, all 5,341 quantified proteins were plotted by their Spearman correlation with SUVmax against statistical significance (Figure 3D). This proteome-wide view shows that the named positive correlates (ATAD1, VPS37A, AGPS, NT5C, ARHGDIA) and negative correlates (PSMD5, SETMAR, RRP15, PES1) occupy the extreme tails of a continuous, approximately symmetric distribution.

Given the small sample size, the stability of these correlations was assessed using exact permutation tests and leave-one-patient-out (LOPO) analyses. The top positive correlations were robust: exact two-sided permutation P-values were 0.0004 for ATAD1, VPS37A and AGPS and 0.0011 for ARHGDIA (n=8). Under LOPO, the three top correlates remained at $r_s \geq 0.96$ when any single patient was removed. ARHGDIA remained at $r_s \geq 0.93$ throughout LOPO. Non-parametric bootstrap 95% confidence intervals (5,000 resamples) were [0.73, 1.00] for ATAD1/AGPS, [0.79, 1.00] for VPS37A and [0.62, 1.00] for ARHGDIA. By contrast, the ERBB2–SUVmax association was not robust (permutation P = 0.67; LOPO r_s ranging from −0.04 to +0.61), consistent with the absence of a correlation between total HER2 and SUVmax. These analyses indicate that the SUVmax-proteome associations are not driven by any single patient and are robust.

Pathway and transcription factor enrichment analysis of the 259 positively correlated proteins ($r \geq 0.70$) and 109 negatively correlated proteins ($r \leq -0.70$) provided a framework that grouped the top SUVmax correlates into three convergent functional themes (Figure 4A): (1) Endocytic recycling and vesicle transport: Two of the top enriched GO Biological Process were "Vesicle-mediated transport to plasma membrane" (adjusted P = 0.0024) and "Endocytic recycling" (adjusted P = 0.0087). These processes are involved in returning internalized receptors to the cell surface and thereby sustain surface-accessible HER2 available to the tracer [16]. (2) Biosynthesis of peroxisome-derived lipids: GO Cellular Component analysis showed significant enrichment of the "Peroxisome" (adjusted P = 0.0015), where ether lipid biosynthesis is catalyzed by AGPS [21]. AGPS ranked as the top SUVmax correlate ($r_s = 0.976$) and was the strongest LF3-loaded lipid metabolism protein (scaled weight = 0.2463). (3) Cytoskeletal remodeling and focal adhesion: GO Cellular Component analysis also enriched for "Focal Adhesion" (adjusted P = 0.0007), containing proteins regulated by ARHGDIA (Rho GDI alpha; SUVmax correlation $r_s = 0.952$, LF3 scaled weight = 0.4749) [22]. Additional top scorers included ATAD1 (AAA+ ATPase) and NT5C (cytosolic 5'-nucleotidase) which showed high SUVmax correlations ($r_s = 0.976$ and 0.952, respectively).ATAD1 has a part in regulating the mitochondrial and peroxisomal membrane protein homeostasis [23] while NT5C regulates intracellular nucleotide pools [24]. Although these proteins have no established association with HER2 surface presentation, their high SUVmax correlations may reflect cellular adaptations linked to HER2-driven metabolic demands [25].Transcription factor enrichment of the positive correlates identified USF1 (adjusted $P = 7.67 \times 10^{-8}$) and USF2 (adjusted $P = 1.59 \times 10^{-7}$). These helix-loop-helix factors are established regulators of lipogenic gene networks [26] and could be involved in the ether lipid synthesis pathway represented by AGPS. The factors TAF1, YY1, and ZBTB7A were also strongly enriched (each adjusted $P = 3.35 \times 10^{-6}$).

In contrast, the negatively correlated proteins (enriched in low-uptake tumors) (Figure 4B), pointed to protein-synthesis and cell-matrix-attachment machinery. "Maturation of LSU-rRNA" (adjusted P = 0.0040; NIFK, PES1, RPL7L1, RRP15) which is involved in protein synthesis machinery [27]. Alongside it, a cluster of adhesion/cytoskeleton terms was co-enriched: Cell-Substrate Junction (adjusted P = 0.0013), Focal Adhesion (0.0015), Vesicle (0.0015) and Cytoskeleton (0.0025). These cell-matrix-adhesion terms appear among both the positive and negative correlates (with largely non-overlapping gene sets), indicating that adhesion programs are remodelled rather than uniformly gained or lost with PET uptake. Transcription Factor enrichment showed that there are significantly more UBTF target genes (adjusted P = 0.0027) among the negatively SUVmax-correlated proteins. UBTF regulates ribosomal transcription [28]. Full enrichment results, including FDR-corrected p-values and key overlapping genes for the top positively and negatively enriched terms, are provided in Supplementary Tables 1 and 2.

Exploratory Radiomics Correlates of Proteomics ERBB2 (HER2) Abundance

Post-hoc analysis of the radiomics view revealed that the ERBB2-associated LF1 was underpinned by specific CT texture features that correlated strongly with tissue ERBB2 protein levels. PCA of the radiomics features showed that PC1 explained 39.7% of the variance, while PC2 explained 23.1%. PC1 showed a correlation with proteomics ERBB2 expression (r_s = 0.857, uncorrected P = 0.024, FDR-corrected-P = 0.09). However, due to the small sample size, the corrected p-value does not reach statistical significance. In contrast, PC1 was not significantly correlated with SUVmax (r_s = 0.100, uncorrected p=0.80, FDR-corrected-P = 1.000) or IHC score (r_s = 0.186, uncorrected P = 0.63, FDR-corrected-P = 1.000). Hierarchical clustering of the top 100 most variable radiomics features grouped the patients into three main clusters (Figure 5A): Cluster 1 containing Patient 4 alone, Cluster 2 containing Patient 5 and Patient 8, and Cluster 3 containing the remaining patients (Patients 1, 2, 3, 7, 9, 10). Patient 4 clustered as a stark outlier due to an exceptionally large tumor volume (61,455 voxels vs. a median of 1,449 voxels for the rest of the cohort), which confounded size-dependent Gray Level Size Zone Matrix (GLSZM) features. Cluster 2 grouped Patients 5 and 8 together, who both have high SUVmax.

Unbiased feature-level correlation analysis identified 5 radiomics features with perfect monotonic correlations (r_s = 1.0) with ERBB2 proteomics across the overlapping cohort (N=7) (Table 4, Figure 5B). Feature names, raw and FDR-corrected p-values are reported in Table 4. These included wavelet-HLL_firstorder_Minimum (r_s= 1.0), gradient_glszm_SmallAreaEmphasis (r_s = -1.0), and gradient_glszm_SmallAreaHighGrayLevelEmphasis (r_s= -1.0). These strong correlations should be considered hypothesis-generating, due to the limited sample size. As far as correlation between radiomics features and IHC or SUVmax is concerned, no individual features survived FDR correction. The top feature for SUVmax was log-sigma-5-0-mm-3D_glcm_ClusterShade (r_s = 0.929, FDR-corrected-P = 0.276). For IHC score, the top correlate

was wavelet-LHH_glszm_SmallAreaLowGrayLevelEmphasis (r_s= -0.894, FDR-corrected-P = 1.000). While these features represent strong correlations (r_s), the high-dimensional multiple testing penalty (2,046 features) on a small sample size (N=9) prevents them from reaching FDR-corrected significance.

For Patient 5 (missing proteomics, IHC 0, SUVmax 24.9), pairwise Euclidean distance across the 2,046 features identified Patient 8 (IHC 2+, SUVmax 33.4) as the nearest neighbor (distance = 39.18 vs. a cohort average of 68.32). This radiomics similarity is consistent with their high metabolic activity (both being high SUVmax patients). However, looking specifically at the Z-scores of the top ERBB2-predicting radiomics features, Patient 5 had a low Z-score for wavelet-LLL_glrlm_LongRunLowGrayLevelEmphasis (-0.856, second lowest in the cohort, nearly identical to the lowest patient, Patient 7, who had a Z-score of -0.856), which is positively correlated with ERBB2. At the same time, Patient 5 had a very high Z-score for gradient_glszm_SmallAreaEmphasis (+1.317, second highest in the cohort), which is negatively correlated with ERBB2. This is consistent with Patient 5's pathological status of HER2 IHC 0. This is presented as an illustrative case rather than independent validation of the hypothesis.

Multiple Testing and Statistical Robustness

Under the BH-FDR procedure at $P < 0.05$, no SUVmax correlations reached significance across the 5,341 proteins tested and no correlation could meet the Bonferroni threshold ($P < 9.36 \times 10^{-6}$), as detailed in Methods. For TBR, the top five proteins (AAR2, VPS37A, PLCG2, CTSA, ITGA1) reached borderline significance (FDR-corrected-P = 0.050) (Table 2). No IHC correlations survived FDR correction (top FDR-corrected-P = 0.845).

However, the effect sizes for the top correlations were very large. All top 10 positively correlated proteins exceeded Cohen's threshold for a large effect ($r > 0.50$), and the 95% confidence intervals for the top three proteins ($r = 0.976$) excluded correlations below $r = 0.87$, which is remains a very large effect. The lower bound of the 95% CI for the fifth-ranked protein ($r = 0.952$) was $r = 0.75$. By contrast, the 95% CI for ERBB2 ($r = 0.191$) spanned from -0.59 to +0.79, encompassing trivial and even inverse correlations. These results illustrate the distinction between statistical significance (which depends on sample size and multiple testing burden) and effect size (which reflects the magnitude of association). In this small discovery cohort, the large correlations observed for AGPS and ARHGDIA, supported by their biological plausibility and by their strong loading on the MOFA SUVmax-associated latent factor, suggest viable hypotheses that require testing in a larger validation cohort.

Discussion

In this multi-omics analysis of paired tumor biopsies and co-registered imaging from patients with HER2-low metastatic breast cancer undergoing [^{68}Ga]Ga-ABY-025 PET/CT, four principal observations are reported. First, total HER2 abundance correlated neither with IHC scores nor with [^{68}Ga]Ga-ABY-025 uptake, replicating the well-documented discordance between bulk receptor measurements and in vivo tracer accumulation [29]. SUVmax is a composite measure influenced by perfusion, tracer delivery, lesion size, motion artefacts, image noise, partial-volume effects and binding kinetics, and is therefore interpreted here as in vivo tracer accumulation rather than a direct readout of surface-accessible receptor density. Second, Multi-Omics Factor Analysis (MOFA) identified two separate latent factors: a radiomics-linked latent factor (LF1) that captured absolute tissue HER2 density and a proteomics-linked latent factor (LF3) that captured the functional membrane machinery governing surface HER2 accessibility. Third, a proteomic/pathway enrichment analysis which shed light on the role of proteins involved in the membrane machinery (LF3). These included proteins involved in membrane lipid composition (AGPS), receptor endocytic recycling, and cytoskeletal remodeling (ARHGDIA), all of which appear correlated with SUVmax. Fourth, post-hoc radiomics analysis identified a small number of high-frequency wavelet and gradient texture features with near-perfect rank correlations with tissue HER2 levels. This exploratory finding requires independent validation before it can be considered a non-invasive indicator of receptor density. Together, these findings support a model in which [^{68}Ga]Ga-ABY-025 PET uptake reflects surface-accessible receptor density regulated by membrane microenvironment dynamics, rather than total cellular HER2 content (Figure 6)

The separate latent factors that MOFA identified for receptor density and surface accessibility are biologically intuitive since [^{68}Ga]Ga-ABY-025 is a small (~7 kDa) affibody that binds a distinct epitope on the HER2 extracellular domain [15] and because it circulates systemically, only binds receptors physically exposed on the outer plasma membrane, while internalized receptors are invisible [16]. Cell-model studies show that HER2-overexpressing lines offset endocytosis with rapid recycling, whereas HER2-low cells route internalized receptors more efficiently to lysosomal degradation [16]. Our data suggests that a similar dynamic operates in human metastases, and that the recycling-degradation balance captured by LF3 is a stronger determinant of PET signal than absolute receptor number. Discordant cases illustrate this: Patient 10 had the highest HER2 abundance but only moderate SUVmax, consistent with high total receptor density yet limited surface accessibility. Patient 8 showed the converse (highest SUVmax with below average HER2 levels), although their retrospective biopsy introduces temporal uncertainty.

Pathway enrichment of LF3-loaded proteins supports a model for surface HER2 retention (Figure 6). Firstly, in line with previous work demonstrating dynamic HER2 recycling [30], endocytic recycling and vesicle mediated transport to the plasma membrane may also contribute to maintaining HER2 surface availability. Secondly, biosynthesis of peroxisome-

derived lipids implicates AGPS [21], which was a key factor in LF3. These lipids contribute to the structural organization and stability of cholesterol-rich membrane microdomains (lipid rafts) [21], where HER2 is located [31]. Thus, we hypothesize that increased AGPS could be enhancing surface HER2 availability. In line with this, Benjamin et al. showed that AGPS knockdown impairs aggressive breast cancer phenotypes [32]. Thirdly, cytoskeletal remodeling and focal adhesion dynamics may contribute to HER2 surface availability. Focal adhesions are membrane-associated complexes that physically connect the actin cytoskeleton to the extracellular matrix [33]. Patients with elevated ARHGDIA showed enrichment of the focal adhesion pathway, consistent with the role of ARHGDIA in Rho GTPase-mediated regulation of the actin cytoskeleton and cell adhesion processes [22]. Recent work has shown that HER2 associates with focal adhesion complexes, with inhibition of focal adhesion kinases (FAK) impairing HER2 clustering [34] and improving treatment response in HER2+ models [35]. Moreover, disruption of actin polymerization impairs HER2 clustering [34], whereas actin-rich membrane protrusions have been associated with sustained HER2 signaling and reduced HER2 internalization and degradation [36]. Together, these findings suggest that cytoskeletal and adhesion-associated processes influence HER2 membrane organization and, potentially, contribute to sustained surface availability. High ARHGDIA expression has been further linked to better chemotherapy response in invasive ductal cancer [37], possibly reflecting preserved surface receptor availability. Moreover, transcriptional coordination via USF1/USF2, which are established lipogenic regulators [26] and have been implicated in breast cancer [38][39], suggests a system involved with the lipid rafts and membrane. Interestingly, the VPS37A protein, while being strongly positively correlated with SUVmax (r_s=0.9762) and having a weight similar to AGPS and ARHGDIA in LF3 (0.1943), is involved in receptor trafficking and degradation. In breast cancer, VPS37A loss drives EGFR accumulation and poor prognosis [40]. Thus, high VPS37A is unlikely to simply reflect increased surface receptor retention and may instead indicate a more complex relationship between VPS37A-dependent trafficking, tumor metabolic activity and HER2 overexpression [41]

HER2 IHC and PET SUVmax track distinct, non-overlapping proteomics signatures. SUVmax showed stronger association with membrane-organization proteins (AGPS, ARHGDIA), whereas IHC correlated with endocytic and degradative proteins (CLTA, VPS26A, CTSZ). Total ERBB2 (HER2) itself correlated poorly with both. This divergence makes biological sense since PET measures only surface-accessible, tracer-binding receptors. Neither alone is sufficient to predict the other, as also hypothesized by earlier works [17], reinforcing the need for complementary biomarkers, such as the non-invasive radiomics.

While LF3 explains why [^{68}Ga]Ga-ABY-025 PET/CT does not track total ERBB2, LF1 demonstrates that CT radiomics can non-invasively approximate absolute tissue receptor density. Specific high-frequency texture features showed strong rank correlations with ERBB2 proteomics , capturing sub-visual spatial heterogeneity that may scale with target

concentration. However, at n=7 these radiomics features did not survive FDR correction. Patient 5 lacked proteomics but showed high PET uptake (SUVmax 24.9), and their candidate ERBB2-correlated radiomics profile nonetheless clustered with low-receptor-density patients, consistent with their IHC score of 0. This raises the possibility that radiomics could help decouple absolute receptor density from perfusion effects that drive high [^{68}Ga]Ga-ABY-025 uptake, pending validation in a larger cohort. Our findings extend emerging radiogenomic literature linking CT texture to HER2 status [42][43] with exploratory correlations against mass spectrometry-quantified ERBB2 in the same tumors.

Our findings shed light on prior [^{68}Ga]Ga-ABY-025 PET/CT discordances including moderate SUVmax-IHC correlation [17], HER2-low "false-positive" PET lesions [13] and frequent biopsy-imaging mismatches [44]. This work aims to offer a mechanistic explanation in which [^{68}Ga]Ga-ABY-025 uptake in PET/CT reflects surface-accessible HER2 (LF3), while biopsy IHC (a membrane-staining assay) and bulk proteomics reflect aggregate receptor abundance and are themselves influenced by tumor purity, stroma and sampling (LF1). This is particularly relevant for HER2-low disease, where small differences in surface density amplified by lipid raft or cytoskeletal machinery could determine PET visibility and ADC responsiveness. Recent proteogenomic subtyping underscores this heterogeneity [45]. If uptake depends on surface accessibility rather than aggregate receptor abundance, a single biopsy provides limited information about the receptor pool available to a circulating ADC (such as T-DXd), whereas PET assesses this property across all lesions non-invasively. This hypothesis is currently under prospective evaluation in an ongoing trial. The LF1 radiomics signature is complementary, as it may permit approximation of tissue HER2 abundance where biopsy is unavailable.

This study has several limitations. The sample sizes for the proteomic (n = 8) and radiomic (n = 9) analyses were limited. Accordingly, these findings should be considered exploratory and hypothesis-generating and require validation in larger, independent cohorts. Radiomics is subject to volume confounding and potential spatial mismatch, while Patient 8's retrospective biopsy introduces temporal uncertainty. Future work should validate these protein/radiomics candidates in larger cohorts using proteomics. Because the cohort originated from a Phase II study and was small (n = 8), the number of events was insufficient to fit a formal multivariable model, and candidate confounders were instead evaluated individually. In low-order partial correlation analyses adjusting for these confounders one at a time (e.g. ER and Ki-67), the leading associations were largely unchanged (AGPS partial rs ≈ 0.94), indicating that they were not explained by any single measured confounder. A further candidate confounder was genomic co-linearity as ERBB2 and ARHGDIA both map to chromosome 17q, but they lie 42 Mb apart and their abundances were uncorrelated across patients (rs = −0.02, P = 0.96), making shared copy-number gain an unlikely explanation. Notably, tracer uptake co-varied with clinical phenotype as SUVmax was higher in hepatic than in extrahepatic lesions. Because the leading proteins covary with the same variables, the proteomics associations reported here may also reflect tumor phenotype. In addition, all molecular data derive from a single biopsied lesion per patient and therefore might not capture the inter-lesional heterogeneity that whole-body imaging is intended to address. Finally, this cohort has no data

linking [^{68}Ga]Ga-ABY-025 PET/CT to T-DXd response, and that question is being addressed prospectively in our ongoing HER2-Ex PET trial. Residual confounding by lesion biology/location nonetheless cannot be excluded and should be addressed in a larger cohort powered for multivariable adjustment.

In summary, this multi-omics pilot study of HER2-low metastatic breast cancer demonstrates that [^{68}Ga]Ga-ABY-025 uptake in PET/CT examination is not driven by total cellular HER2 abundance, but rather by proteins linked to surface receptor accessibility, membrane organization, lipid composition, cytoskeletal remodeling, and endocytic recycling. MOFA independently separated this functional surface-accessibility axis from a radiomics-linked axis reflecting absolute HER2 density. Although definitive statistical significance was not always reached due to the small sample size of this Phase II study, the large effect sizes, biological coherence, and convergence across proteomic, pathway and radiomics analyses generate testable hypotheses for future validation. If confirmed in larger studies, LF1-linked radiomic features may also enable non-invasive estimation of tissue HER2 abundance where biopsy is unavailable.

Declarations

Ethics approval

This study was performed in accordance with the ethical principles of the Declaration of Helsinki and the ICH Good Clinical Practice guidelines. The trial was approved by the Swedish Ethical Review Authority (Etikprövningsmyndigheten) and the Swedish Medical Products Agency (Läkemedelsverket) (Dnr 5.1-2022-58345; EU CT 2022-500448-39-00).

Consent to participate

Written informed consent was obtained from all individual participants included in the study prior to any study-specific procedures.

Consent for publication

All participants consented, as part of the written informed consent, to the publication of study results in anonymised form. The manuscript contains no information or images that could identify individual participants.

Competing interests

RA reports fees paid to the institution for educational activities, research projects and advisory boards from Roche, Astra Zeneca, Exact Sciences, Seagen, Novartis. All other authors have declared that no competing interests exist.

Funding

This study is funded by a grant from Swedish Breast Cancer Society 2023 to RA. The ABY-025 precursor was kindly provided by Affibody Sweden AB. The funders have not had a direct role in the design of the study and collection, analysis, or interpretation of data.

Authors contributions

Trial design: RAl, JL, AT, TT

Trial funding: RAl, RAx

Protocol preparation: RAl, RAx

Data collection: KV, HJ, M, LFG, SaB, TN, RAl, AT, RAx,

Data analysis: KV, HJ, MZ, LFG, TN, MH, EV, MEK, AT

Manuscript writing: all authors.

Acknowledgements

We are grateful to the dedicated professionals at the Departments of Radiopharmacy, Nuclear Medicine, and Breast Clinic at the Karolinska university hospital in Stockholm for their invaluable contributions. We also acknowledge the support of the Center for Clinical Cancer Trials and the Clinical Trial Office at Karolinska University Hospital, Affibody AB for generously providing the ABY-025 precursor and SciLifeLab for performing the proteomics analyses. Most importantly, we are deeply indebted to the patients who chose to participate in this trial.

Data availability statement

Data will be shared upon reasonable request to the corresponding author.

References

1. Tarantino P, Hamilton E, Tolaney SM, et al (2020) HER2-Low Breast Cancer: Pathological and Clinical Landscape. J Clin Oncol 38:1951–1962
2. Modi S, Jacot W, Yamashita T, et al (2022) Trastuzumab Deruxtecan in Previously Treated HER2-Low Advanced Breast Cancer. New England Journal of Medicine 387:9–20
3. Bardia A, Hu X, Dent R, et al (2024) Trastuzumab Deruxtecan after Endocrine Therapy in Metastatic Breast Cancer. New England Journal of Medicine 391:2110–2122
4. FDA approves fam-trastuzumab deruxtecan-nxki for unresectable or metastatic HR-positive, HER2-low or HER2-ultralow breast cancer | FDA. https://www.fda.gov/drugs/resources-information-approved-drugs/fda-approves-fam-trastuzumab-deruxtecan-nxki-unresectable-or-metastatic-hr-positive-her2-low-or-her2. Accessed 8 Jul 2026
5. Nicolò E, Boscolo Bielo L, Curigliano G, Tarantino P (2023) The HER2-low revolution in breast oncology: steps forward and emerging challenges. Ther Adv Med Oncol 15:
6. Wolff AC, Elizabeth Hale Hammond M, Allison KH, et al (2018) Human Epidermal Growth Factor Receptor 2 Testing in Breast Cancer: American Society of Clinical Oncology/College of American Pathologists Clinical Practice Guideline Focused Update. J Clin Oncol 36:2105–2122
7. Agostinetto E, Rediti M, Fimereli D, et al (2021) HER2-Low Breast Cancer: Molecular Characteristics and Prognosis. Cancers (Basel) 13:
8. Gong C, Liu C, Tao Z, et al (2022) Temporal Heterogeneity of HER2 Expression and Spatial Heterogeneity of 18F-FDG Uptake Predicts Treatment Outcome of Pyrotinib in Patients with HER2-Positive Metastatic Breast Cancer. Cancers (Basel) 14:3973
9. Miglietta F, Griguolo G, Bottosso M, et al (2021) Evolution of HER2-low expression from primary to recurrent breast cancer. npj Breast Cancer 2021 7:1 7:137-
10. Sörensen J, Velikyan I, Sandberg D, et al (2016) Measuring HER2-Receptor Expression In Metastatic Breast Cancer Using [68Ga]ABY-025 Affibody PET/CT. Theranostics 6:262–271
11. Karakas C, Tyburski H, Turner BM, et al (2023) Interobserver and Interantibody Reproducibility of HER2 Immunohistochemical Scoring in an Enriched HER2-Low-Expressing Breast Cancer Cohort. Am J Clin Pathol 159:484–491

12. Modi S, Park H, Murthy RK, et al (2020) Antitumor Activity and Safety of Trastuzumab Deruxtecan in Patients With HER2-Low–Expressing Advanced Breast Cancer: Results From a Phase Ib Study. Journal of Clinical Oncology 38:1887

13. Burén S af, Romdhani NS, Ulaner G, et al (2026) HER2-targeted PET/CT in breast cancer: a systematic review of lesion-level concordance with pathology. Eur J Radiol 202:112961

14. Eissler N, Altena R, Alhuseinalkhudhur A, et al (2024) Affibody PET Imaging of HER2-Expressing Cancers as a Key to Guide HER2-Targeted Therapy. Biomedicines 12:

15. Sörensen J, Sandberg D, Sandström M, et al (2014) First-in-Human Molecular Imaging of HER2 Expression in Breast Cancer Metastases Using the 111In-ABY-025 Affibody Molecule. Journal of Nuclear Medicine 55:730–735

16. Ram S, Kim D, Ober RJ, Ward ES (2014) The level of HER2 expression is a predictor of antibody-HER2 trafficking behavior in cancer cells. MAbs 6:1211

17. Altena R, Burén S, Blomgren A, et al (2024) Human Epidermal Growth Factor Receptor 2 (HER2) PET Imaging of HER2-Low Breast Cancer with [68Ga]Ga-ABY-025: Results from a Pilot Study. Journal of Nuclear Medicine 65:700–707

18. Santinha J, Pinto dos Santos D, Laqua F, et al (2024) ESR Essentials: radiomics—practice recommendations by the European Society of Medical Imaging Informatics. Eur Radiol 35:1122

19. Argelaguet R, Velten B, Arnol D, et al (2018) Multi-Omics Factor Analysis-a framework for unsupervised integration of multi-omics data sets. Mol Syst Biol 14:

20. Argelaguet R, Arnol D, Bredikhin D, et al (2020) MOFA+: a statistical framework for comprehensive integration of multi-modal single-cell data. Genome Biol 21:111

21. Dean JM, Lodhi IJ (2017) Structural and functional roles of ether lipids. Protein Cell 9:196

22. Garcia-Mata R, Boulter E, Burridge K (2011) The “invisible hand”: regulation of RHO GTPases by RHOGDIs. Nature Reviews Molecular Cell Biology 2011 12:8 12:493–504

23. Yan HH, He JJ, Fu C, et al (2025) ATAD1 Regulates Neuronal Development and Synapse Formation Through Tuning Mitochondrial Function. Int J Mol Sci 26:44

24. Gene - NT5C. https://maayanlab.cloud/Harmonizome/gene/NT5C. Accessed 13 Jul 2026

25. Holloway RW, Marignani PA (2021) Targeting mTOR and Glycolysis in HER2-Positive Breast Cancer. Cancers 2021, Vol 13, Page 2922 13:2922

26. Rada-Iglesias A, Ameur A, Kapranov P, et al (2008) Whole-genome maps of USF1 and USF2 binding and histone H3 acetylation reveal new aspects of promoter structure and candidate genes for common human disorders. Genome Res 18:380

27. Bohnsack KE, Bohnsack MT (2019) Uncovering the assembly pathway of human ribosomes and its emerging links to disease. EMBO J 38:EMBJ2018100278-

28. Sanij E, Diesch J, Lesmana A, et al (2015) A novel role for the Pol I transcription factor UBTF in maintaining genome stability through the regulation of highly transcribed Pol II genes. Genome Res 25:201–212

29. Lawal IO, Li X, Sakach EA, et al (2026) Negative 18 F-FES PET/CT Despite Estrogen Receptor Positivity by Immunohistochemistry. Clin Nucl Med 51:e244–e246

30. Austin CD, De Mazière AM, Pisacane PI, et al (2004) Endocytosis and Sorting of ErbB2 and the Site of Action of Cancer Therapeutics Trastuzumab and Geldanamycin. Mol Biol Cell 15:5268

31. Jeong J, Shin JH, Li W, et al (2021) MAL2 mediates the formation of stable HER2 signaling complexes within lipid raft-rich membrane protrusions in breast cancer cells. Cell Rep 37:110160

32. Benjamin DI, Cozzo A, Ji X, et al (2013) Ether lipid generating enzyme AGPS alters the balance of structural and signaling lipids to fuel cancer pathogenicity. Proc Natl Acad Sci U S A 110:14912–14917

33. Kuo JC (2013) Mechanotransduction at focal adhesions: integrating cytoskeletal mechanics in migrating cells. J Cell Mol Med 17:704

34. Wang SE, Xiang B, Zent R, et al (2009) Transforming growth factor β induces clustering of HER2 and integrins by activating Src-FAK and receptor association to the cytoskeleton. Cancer Res 69:475

35. Lazaro G, Smith C, Goddard L, et al (2013) Targeting focal adhesion kinase in ER+/HER2+ breast cancer improves trastuzumab response. Endocr Relat Cancer 20:691–704

36. Jeong J, Kim W, Kim LK, et al (2017) HER2 signaling regulates HER2 localization and membrane retention. PLoS One 12:e0174849

37. Ronneburg H, Span PN, Kantelhardt E, et al (2010) Rho GDP dissociation inhibitor alpha expression correlates with the outcome of CMF treatment in invasive ductal breast cancer. Int J Oncol 36:379–386

38. Mackay A, Jones C, Dexter T, et al (2003) cDNA microarray analysis of genes associated with ERBB2 (HER2/neu) overexpression in human mammary luminal epithelial cells. Oncogene 22:2680–2688

39. Wang D, Jin X, Lei M, et al (2022) USF1-ATRAP-PBX3 Axis Promote Breast Cancer Glycolysis and Malignant Phenotype by Activating AKT/mTOR Signaling. Int J Biol Sci 18:2452

40. Tomasich E, Topakian T, Heller G, et al (2021) Loss of HCRP1 leads to upregulation of PD-L1 via STAT3 activation and is of prognostic significance in EGFR-dependent cancer. Translational Research 230:21–33

41. Xu J, Yang W, Wang Q, et al (2014) Decreased HCRP1 expression is associated with poor prognosis in breast cancer patients. Int J Clin Exp Pathol 7:7915

42. Fan Y, Pan X, Yang F, et al (2022) Preoperative Computed Tomography Radiomics Analysis for Predicting Receptors Status and Ki-67 Levels in Breast Cancer. Am J Clin Oncol 45:526

43. Yang X, Wu L, Zhao K, et al (2020) Evaluation of human epidermal growth factor receptor 2 status of breast cancer using preoperative multidetector computed tomography with deep learning and handcrafted radiomics features. Chin J Cancer Res 32:175–185

44. Alhuseinalkhudhur A, Lindman H, Liss P, et al (2023) Human Epidermal Growth Factor Receptor 2-Targeting [68Ga]Ga-ABY-025 PET/CT Predicts Early Metabolic Response in Metastatic Breast Cancer. J Nucl Med 64:1364–1370

45. Xu S, Yu K, Liu L, et al (2026) Proteogenomic Characterization Reveals Subtype-Specific Therapeutic Potential for HER2-Low Breast Cancer. Adv Sci (Weinh) 13:

Tables and figures

Table 1. Patient characteristics, tumor biology, HER2 IHC score, SUVmax, and ERBB2 (HER2) proteomics levels.

	Tumor Biopsy		HER2-PET		Proteomics
Publication ID[17]	Breast cancer type	HER2 IHC	SUVmax	TBR	Proteomics ERBB2 level
Patient 1	Ductal carcinoma	1+	12.9	6.8	495.46
Patient 2	Ductal carcinoma	1+	6.1	2.3	449.60
Patient 3	Ductal carcinoma	2+	28.7	15.9	615.34
Patient 6 (A)	Lobular carcinoma	0	3.7	1.7	379.41
Patient 6 (B)	Lobular carcinoma	0	3.7	1.7	547.03
Patient 7	Ductal carcinoma	2+	10.3	6.1	202.32
Patient 8	Ductal carcinoma	2+	33.4	15.9	294.37
Patient 9	Ductal carcinoma	2+	19.0	8.3	691.49
Patient 10	Lobular carcinoma	2+	12.0	7.5	1424.09

Table 2. Correlation coefficients between key proteins and PET metrics. Spearman rank correlation is shown with 95% confidence intervals and FDR corrected and uncorrected P-values. Top proteins were selected independently for each metric from the full proteome (5,341 proteins).

Metric / Protein	Spearman r	95% Confidence Interval	Raw P-value	FDR p-value
SUVmax Correlations				
ATAD1	0.9762	[0.870, 0.996]	3.47×10^{-4}	0.62 (n.s.)
VPS37A	0.9762	[0.870, 0.996]	3.47×10^{-4}	0.62 (n.s.)
AGPS	0.9762	[0.870, 0.996]	3.47×10^{-4}	0.62 (n.s.)
NT5C	0.9524	[0.753, 0.992]	7.44×10^{-4}	0.79 (n.s.)
ARHGDIA	0.9524	[0.753, 0.992]	7.44×10^{-4}	0.79 (n.s.)
ERBB2	0.1905	[-0.594, 0.789]	6.51×10^{-1}	0.9729
TBR Correlations				
AAR2	0.9701	[0.839, 0.995]	6.55×10^{-5}	0.0500
VPS37A	0.9701	[0.839, 0.995]	6.55×10^{-5}	0.0500
PLCG2	0.9701	[0.839, 0.995]	6.55×10^{-5}	0.0500
CTSA	0.9701	[0.839, 0.995]	6.55×10^{-5}	0.0500
ITGA1	0.9701	[0.839, 0.995]	6.55×10^{-5}	0.0500
ERBB2	0.3114	[-0.504, 0.833]	4.53×10^{-1}	0.9804
HER2 IHC biopsy score Correlations				
CLTA	0.8660	[0.414, 0.975]	5.42×10^{-3}	0.8451
VPS26A	0.8660	[0.414, 0.975]	5.42×10^{-3}	0.8451
COPRS	0.8660	[0.414, 0.975]	5.42×10^{-3}	0.8451

Metric / Protein	Spearman r	95% Confidence Interval	Raw P-value	FDR p-value
CTSZ	0.8660	[0.414, 0.975]	5.42×10^{-3}	0.8451
KRT8	0.8660	[0.414, 0.975]	5.42×10^{-3}	0.8451
ERBB2	0.1650	[-0.611, 0.779]	6.96×10^{-1}	0.9817

Table 3. Loadings (weights) of top correlated proteins (ATAD1, VPS37A, AGPS and ARHGDIA) and ERBB2 on the three MOFA latent factors. High positive values indicate a positive association between the protein's abundance and the MOFA factors.

Protein	LF1 (ERBB2-associated)	LF2	LF3 (SUVmax-associated)
ERBB2	0.1953	0.0132	-0.1032
ATAD1	-0.0199	0.3404	0.2677
VPS37A	-0.0147	0.2285	0.1943
AGPS	-0.0259	0.2652	0.2463
ARHGDIA	-0.0310	0.3959	0.4749

Table 4. Top Radiomics Features Correlated with ERBB2 Proteomics (N = 7 Patients). Raw p-values are exact two-sided permutation p-values.

Feature Name	Spearman r_s	Raw P-value	FDR-corrected p	Interpretation
wavelet-HLL_firstorder_Minimum	1.000	3.97×10^{-4}	0.15	strong positive correlation
wavelet-HLL_firstorder_Maximum	-1.000	3.97×10^{-4}	0.15	inverse correlation.
wavelet-HLL_firstorder_Range	-1.000	3.97×10^{-4}	0.15	inverse correlation.
gradient_glszm_SmallAreaHighGrayLevelEmphasis	-1.000	3.97×10^{-4}	0.15	inverse correlation.
gradient_glszm_SmallAreaEmphasis	-1.000	3.97×10^{-4}	0.15	inverse correlation.
wavelet-LLL_glrlm_LongRunLowGrayLevelEmphasis	0.964	2.78×10^{-3}	0.341	positive correlation
log-sigma-2-0-mm-3D_firstorder_Range	-0.964	2.78×10^{-3}	0.341	inverse correlation.
squareroot_gldm_SmallDependenceEmphasis	-0.964	2.78×10^{-3}	0.341	inverse correlation

Figure 1. (A) Principal component analysis of the proteomics data. Patient 10 clusters separately due to extreme ERBB2 abundance. Patient 6's biopsy was obtained from a cutaneous metastasis, while the rest came from liver/breast/lymph node metastases. Points are colour-coded by SUVmax. (B) heatmap of the top 100 most variable proteins. Samples are annotated by patient ID

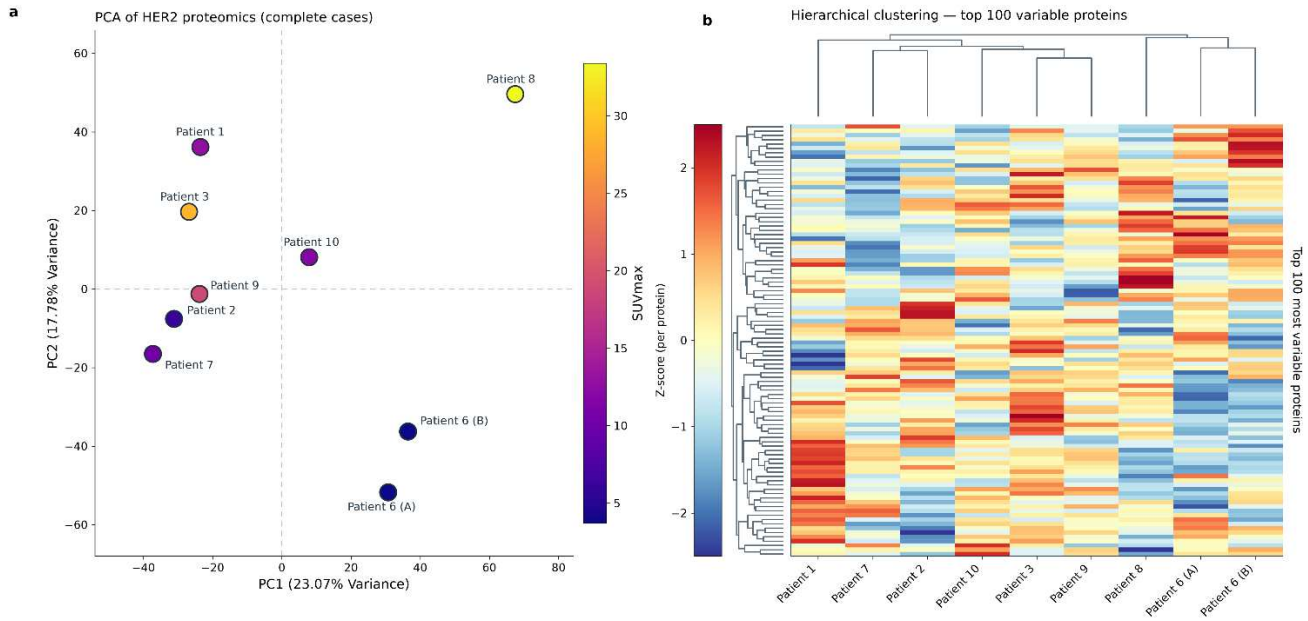


Figure 2. Multi-Omics Factor Analysis (MOFA) integration of Proteomics (5,341 features) and Radiomics (2,046 features) across the matched cohort (N=7 patients). (A) Bar chart showing the percentage of variance explained (R^2%) by each of the three latent factors (LF1–LF3) across the two omics views. (B) Heatmap of Spearman rank correlations (r_s) between latent factors and clinical metrics (SUVmax, TBR, IHC score, and ERBB2 (HER2) proteomics). (C) Latent space scatter plot projecting patients along the LF1 (ERBB2-associated) and LF3 (SUVmax-associated) factor axes. Points are colored by clinical tumor SUVmax. (D) Scatter plot comparing each protein's scaled LF3 loading (x-axis) against its univariate Spearman correlation with SUVmax (y-axis). The prioritized candidate proteins (ARHGDIA, ATAD1, AGPS) are shown in orange, all other proteins are shown in blue. The highest-loading proteins on LF3 are metabolic enzymes (e.g. FAHD2A) and protein regulatory factors (e.g. UBAC1) with weak SUVmax correlations.

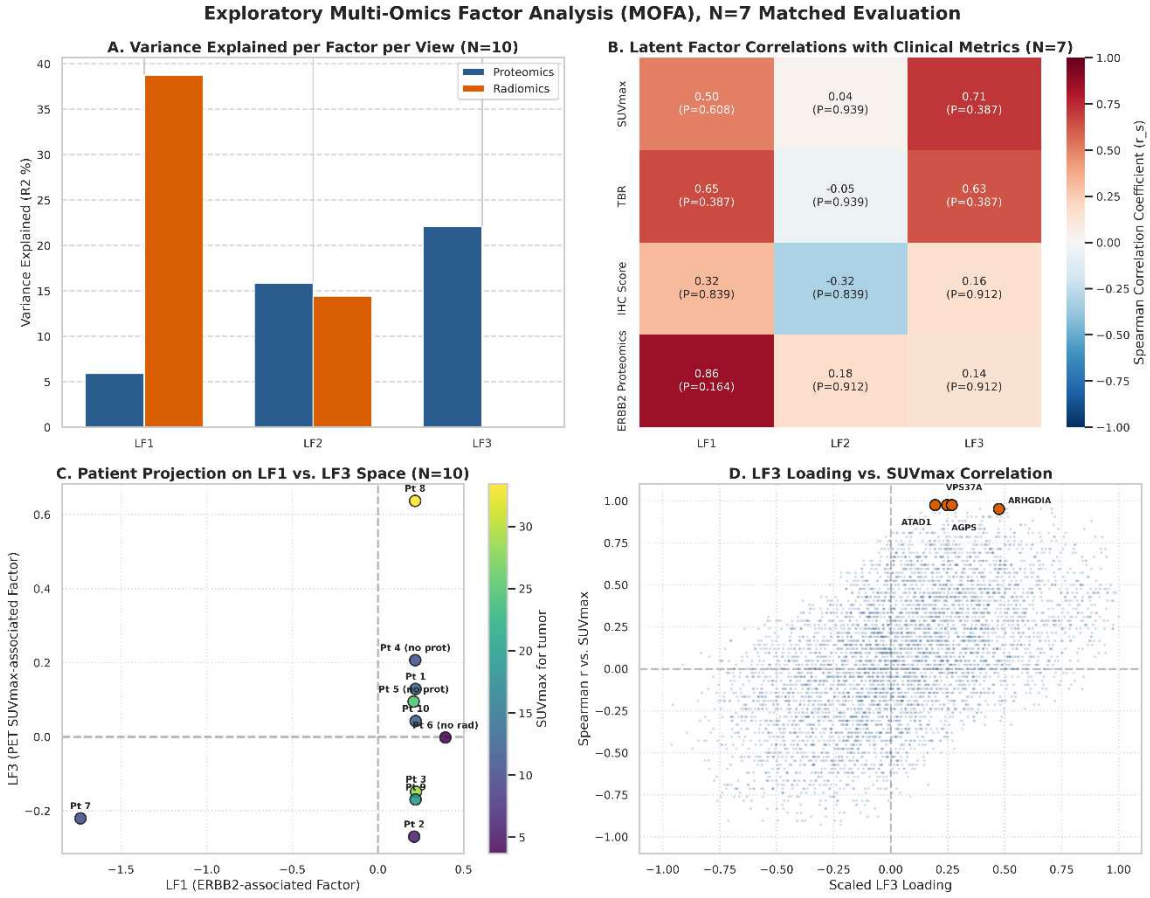


Figure 3. Top proteins correlated with SUVmax. (A) Top 10 positively correlated proteins by Spearman rank correlation. (B) Top 10 negatively correlated proteins. Error bars represent 95% confidence intervals. Dashed line indicates r = 0.50 (Cohen's threshold for large effect size). (C) Heatmap of the top 20 SUVmax-correlated proteins (10 positive, 10 negative). Columns are sorted by patient SUVmax (lowest to highest). Colors represent Z-score expression after log2 transformation. (D) Correlation volcano of all 5,341 quantified proteins, plotting Spearman r_s versus $-\log_{10}(p)$ for the association with SUVmax. Proteins passing the selection thresholds are coloured (red, rs ≥ 0.70, n = 259; blue, rs ≤ −0.70, n = 109); grey points are not selected. Dashed lines mark rs = ±0.70.

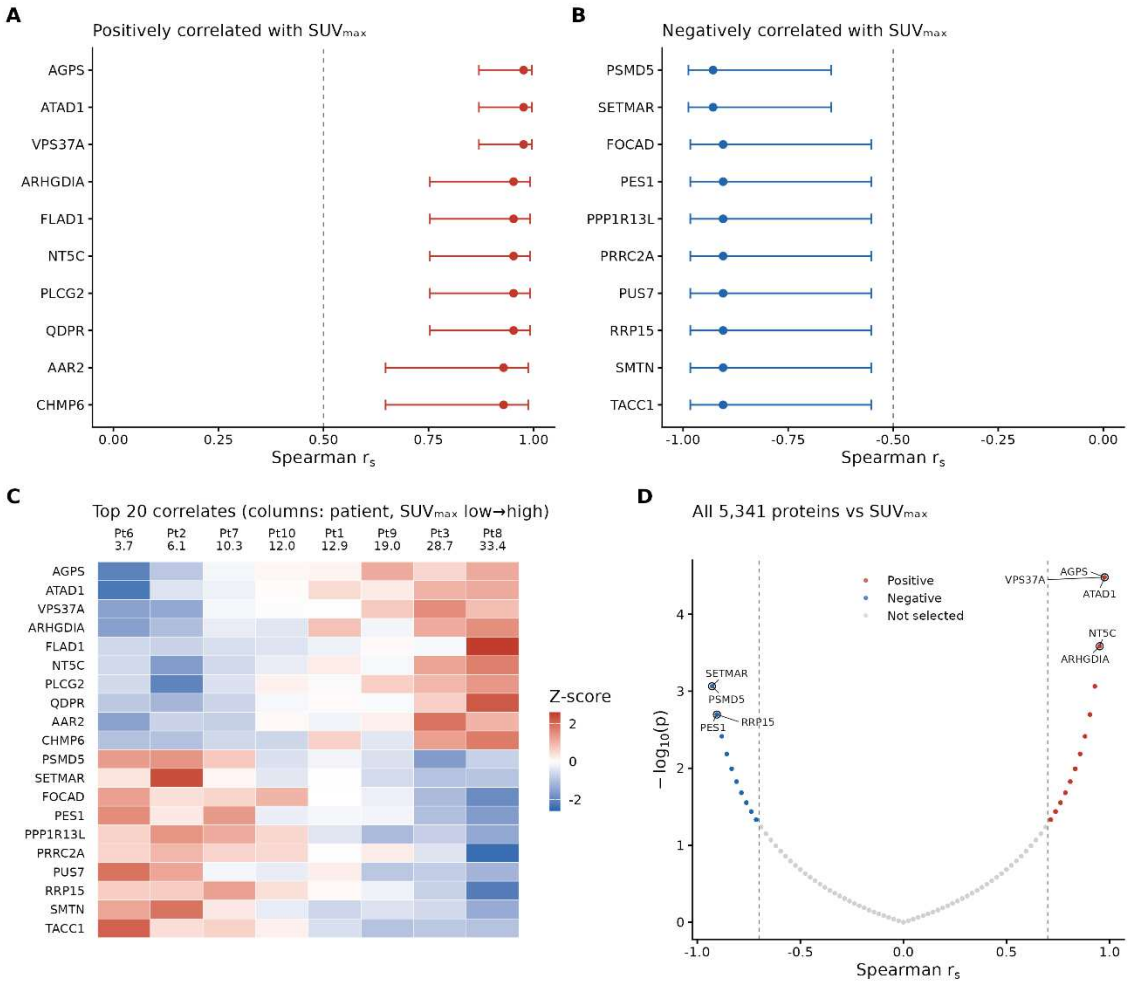


Figure 4. Summary of Enrichment analysis. (A) Positive SUVmax correlates. (B) Negative SUVmax correlates

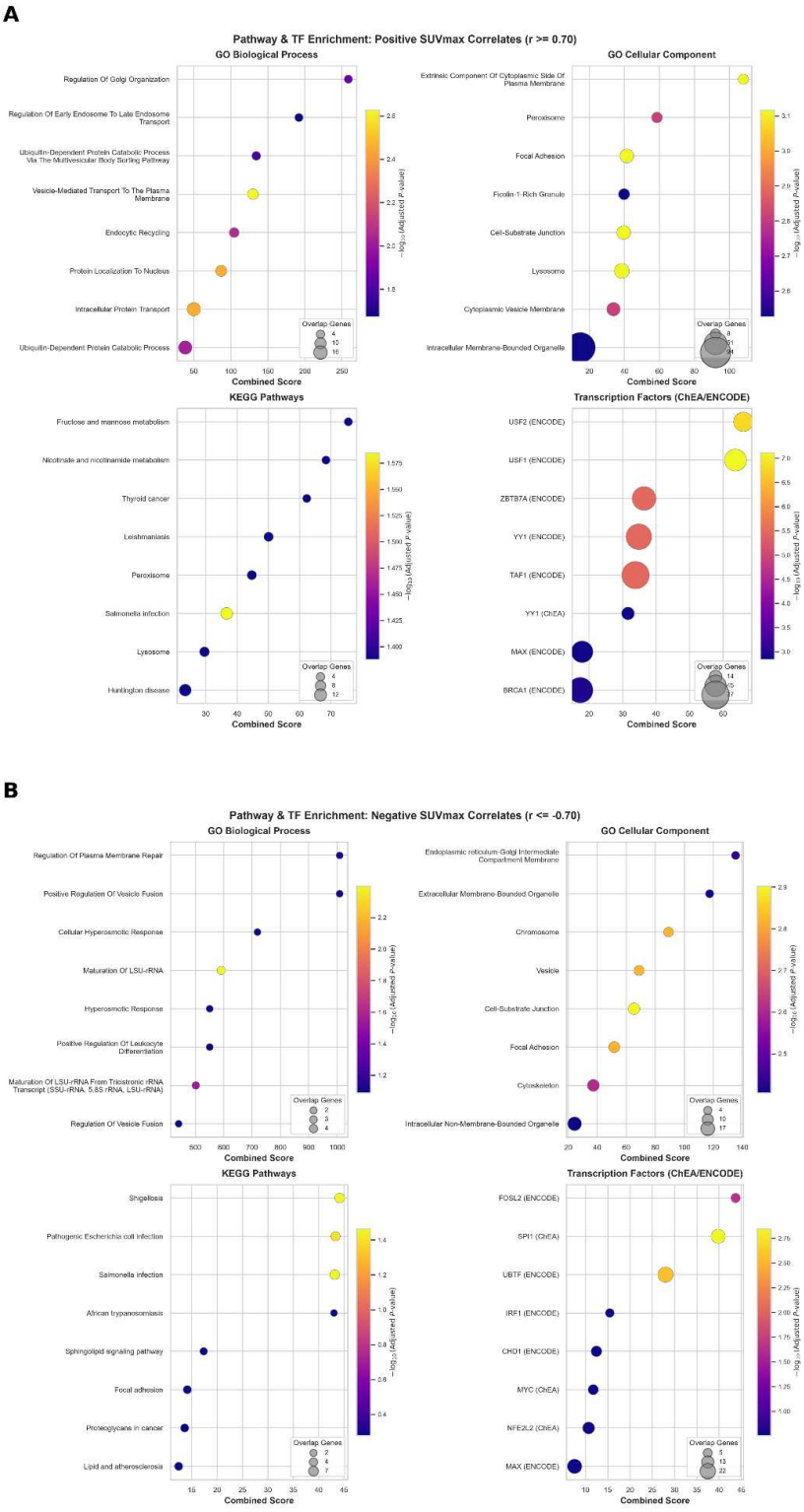


Figure 5. CT radiomics analysis of the HER2-low cohort. (A) Hierarchical clustering dendrogram and heatmap of the top 100 most variable radiomics features. Patient 4 clusters as a distinct outlier due to lesion volume. (B) Correlation scatter plot between one of the top-performing radiomics features `wavelet-HLL_firstorder_Minimum` and mass spectrometry-measured ERBB2 (HER2) proteomics abundance (FDR = 0.15, after correction for 2,046 tested features).

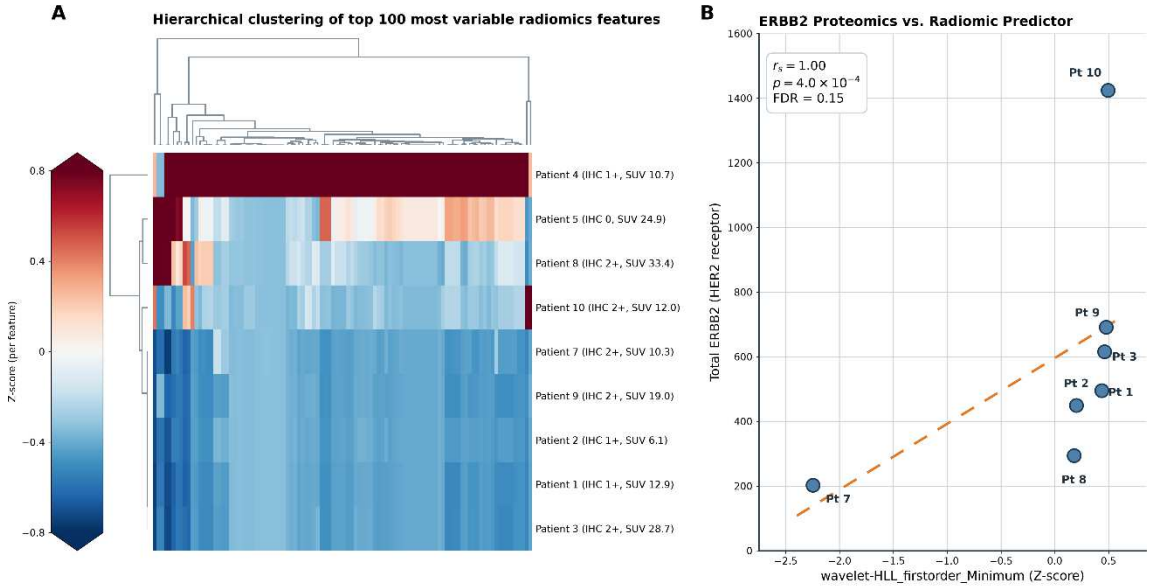
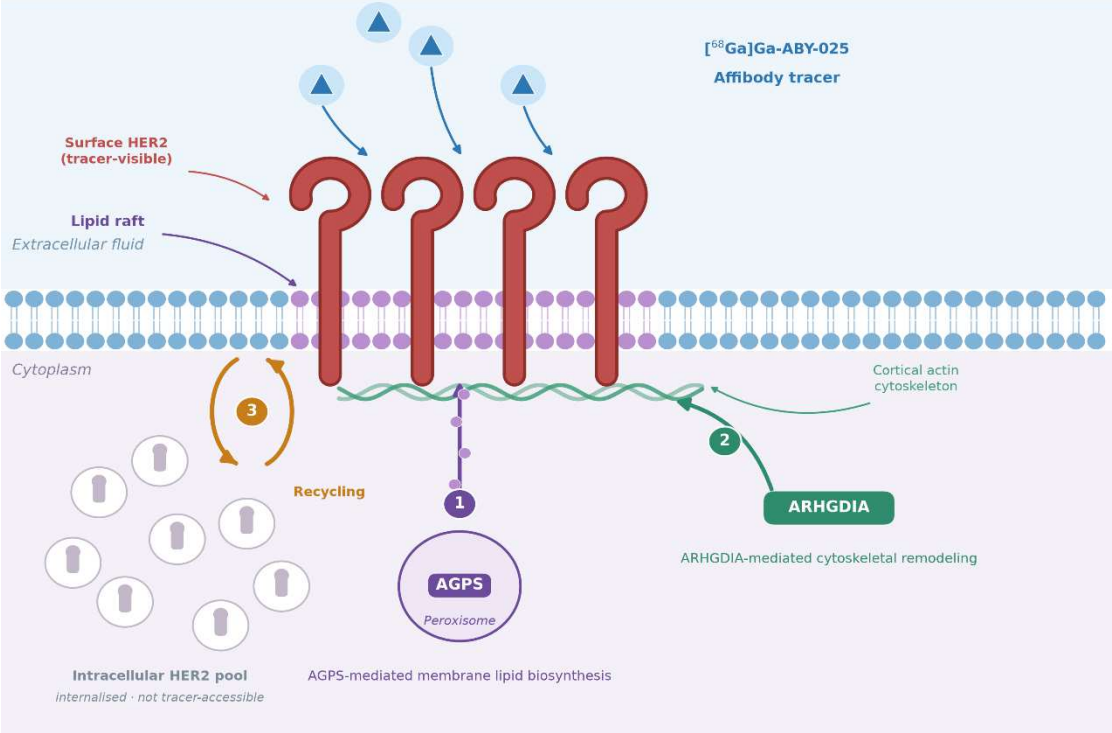


Figure 6. Proposed biological model. Total cellular HER2 abundance (measured by proteomics and IHC) includes intracellular and surface pools. [68Ga]Ga-ABY-025 uptake reflects only surface-accessible HER2, which is regulated by convergent mechanisms: (1) Organization of lipid rafts which contain AGPS-catalyzed ether lipids, (2) ARHGDIA-mediated cytoskeletal remodeling, affecting focal adhesion dynamics and (3) Receptor endocytic recycling. This model could explain why [68Ga]Ga-ABY-025 uptake correlates with membrane microenvironment proteins rather than total ERBB2 (HER2) abundance.



Supplementary Files

This is a list of supplementary files associated with this preprint. Click to download.

- supplementary.docx